ACS APPLIED POLYMER MATERIALS

pubs.acs.org/acsapm Article

Advancing Semiconducting Polymer Patterning: Analysis and Predictive Modeling of Micropatterns Achieved via Photothermal Lithography

Meghna Jha, Joaquin Mogollon Santiana, Megan L. Hong, Emily Vong, Shiva Ahmadi, Harishankar Manikantan, and Adam J. Moulé*

Cite This: ACS Appl. Polym. Mater. 2024, 6, 11302−11311 Read Online

ACCESS | Metrics & More | Article Recommendations | Supporting Information

ABSTRACT: The industrial development of semiconducting polymers (SPs) faces a significant hurdle in the absence of an inexpensive, rapid, and viable patterning technology capable of producing submicron features. In this study, we explore photothermal patterning as a promising technique that leverages the solubility characteristics of SPs to address this challenge. We demonstrate the rapid adaptability of this technique using one of the commercially available direct-write photolithography apparatuses, the Alvéole PRIMO that is commonly found in university clean rooms. Additionally, we developed a predictive model to quantify photothermal dissolution of SPs in solvent mixtures. We successfully determined the depth and width of the resulting patterns and identified the influence of solubility kinetics on heat transfer within the film, tying feature size to laser intensity, dwell time, and solvent quality for two different semiconducting polymers. We then demonstrate the technology by etching complex artwork into SP films with μm lateral resolution and ∼10 nm depth control. Put together, this method and the associated theoretical model set the stage for the development of a cost-effective and rapid photopatterning technology for SPs, opening up possibilities for industrial applications in microfabricating organic electronic devices.

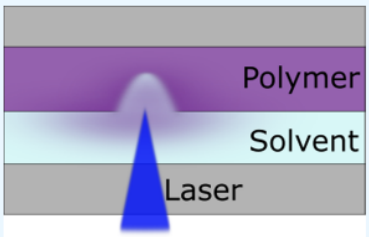

KEYWORDS: *photothermal lithography, semiconducting polymers, μm lateral resolution, nm depth control, Alvéole PRIMO, dissolution temperature, predictive model, large area patterning*

INTRODUCTION

The rate of increase in microprocessor chip speed has doubled roughly every two years for decades as observed by Moore's law. The steady increase in microprocessor speed has largely been the result of miniaturization of individual transistors through improvements in photolithography processing. Photolithography is a multistep chemical processing technique that is used to dope and etch semiconductor domains and to deposit electrodes at desired locations on the chip.[1−3] The worldwide annual investment in photolithography instrumentation increased to over $11 billion/year in 2023.[4] Viability and scalability of any latest semiconducting product will therefore depend largely on how well it integrates with the existing photolithography infrastructure. Utilizing existing photolithography infrastructure for scale-up for upcoming materials with drop-in technology is vastly less expensive and less complicated than developing more instrumentation and processing modalities.

Most photolithography infrastructures are designed for hard semiconducting materials like silicon. Recent research on semiconducting polymers (SPs) demonstrates advantageous material properties like mechanical flexibility, lower environmental toxicity, and superior optoelectronic performance.[5−8] Solution processibility and compatibility with roll-to-roll processing are also huge advantages for SPs compared to hard semiconductors, but progress toward commercial products has been limited because published methods for nano/micropatterning SPs are incompatible with the existing technological infrastructure for electronic devices.[9] Here, we present a chemically nondestructive photopatterning technology capable of laterally and vertically patterning polymer domains with nano/micro resolution that is fully drop-in compatible with existing photolithography infrastructure. We demonstrate high-resolution micropatterning of both p-type and n-type SPs, making this technology an optimal choice for scale-up of future SP devices.

SP micropatterning is an active area of current research with multiple approaches, each with its own limitation associated with soft material processing. Traditional photolithography employs light to modify the solubility of a photoresist and then uses either lift-off or etching methods to pattern the small

Received: June 18, 2024
Revised: August 23, 2024
Accepted: August 26, 2024
Published: September 5, 2024

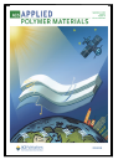

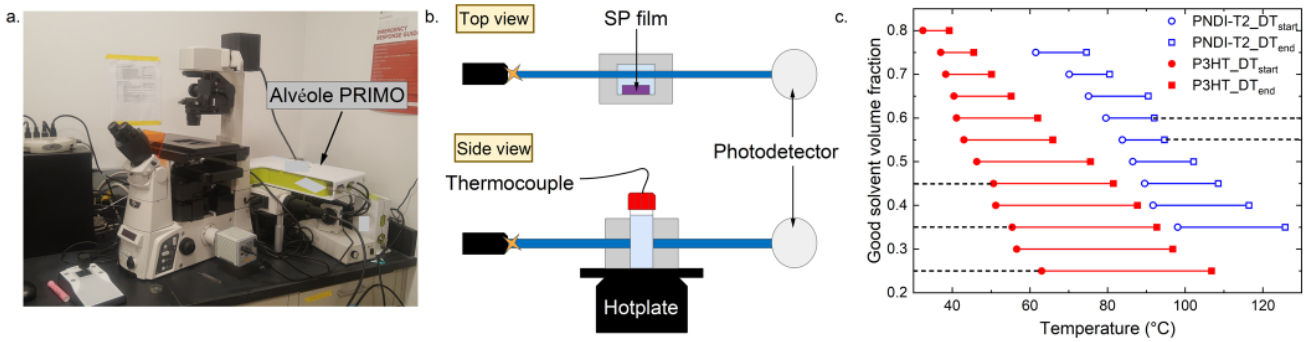

Figure 1. (a) Alvéole PRIMO embedded with a 375 nm laser with contactless and maskless photopatterning. The Alvéole PRIMO is attached to a Nikon eclipse TI microscope. (b) Cartoon schematic of the experimental setup to determine the dissolution temperature. (c) Temperature vs good solvent volume fraction for P3HT (red, filled symbols) and PNDI-T2 (blue, open symbols).

molecule organic semiconductors.[10,11] Photolithography processing steps are usually incompatible with SPs as the SPs and photoresists mix and are soluble in most casting and stripping solvents used in this process.[12] A different approach is to change the chemistry of the SP to enable chemical cross-linking, which makes the SP permanently insoluble.[13] Such a strategy has been widely used for amorphous materials (like emitters for organic light emitting diodes), but the cross-link groups interfere with crystal formation, reducing performance and greatly increasing the difficulty of material processing.[14] Noncontact techniques like inkjet printing operate by ejecting ink droplets from a series of nozzles (with diameter in the range of 9−50 μm) on the substrate.[15−18] These printing techniques are favorable for manufacturing, but result in features that are too large for optical applications.[19,20] And finally, stamping techniques can achieve a higher resolution but the stamp mask often suffers from material deformation and degradation.[21,22] Hence, there is a glaring need for a patterning technique that is compatible with all SPs with no additional chemistry and is noncontact, high-throughput, and high-resolution.

Recent work attempts to address this gap via a contactless, scalable, photopatterning method called projection photothermal lithography.[23] This technique leverages the fact that SPs are soluble in some solvents but insoluble in others. For photothermal lithography, a SP film is exposed to a mixture of a good and a poor solvent that is designed to render the polymer insoluble at room temperature but to enable complete dissolution at an elevated temperature. Subsequently, the SP film is exposed to laser radiation at a wavelength that is strongly absorbed by the SP in its solid state. The absorption of the photons from the laser leads to production of excitons which relax to ground state and through nonemissive processes leads to local heating of the SP. Once the film temperature surpasses the dissolution threshold, the SP dissolves, resulting in the formation of negative patterns.

Using this strategy, Murrey et al. achieved sub-μm resolution with their home-built photothermal patterning setup.[23] However, it is impractical for researchers worldwide to replicate the entire setup, including a microscope, laser, and photomask alignment system. The objective of this study is to evaluate the compatibility of commercially available direct-write photolithography equipment for this process and prove universal replicability. We demonstrate that commercial photolithography equipment can be easily adapted to pattern SPs. In this study, we used the Alvéole PRIMO, which is a commercially available maskless photoaligner designed for biomolecule micropatterning, hydrogel polymerization, and microfabrication, all in a single device.[24−26] We used this apparatus to test the photothermal patterning of both p-type and n-type polymers at various solvent concentrations and laser fluences. We also developed a quasi-steady state model to predict the depth, width, and shape of the negative pattern as a function of the solvent quality, depth of focus, laser fluence, and dwell time. Our results and predictive model demonstrate that photothermal patterning is compatible with available commercial photolithography equipment and that the method can be predictably and universally applied to any SP for electronic device fabrication.

RESULTS AND DISCUSSION

Photothermal Patterning and Solvent Selection. In this study, we used poly(3-hexylthiophene) (P3HT) and poly[*N*,*N*′-bis(2-octyldodecyl)-naphthalene-1,4,5,8-bis-(dicarboximide)-2,6-diyl]-alt-5,5′-(2,2′-bithiophene) (PNDI-T2) as the SPs of interest. These polymers are significantly different because P3HT is a p-type homopolymer that is highly crystalline, orients edge-on to the substrate, and absorbs poorly at 375 nm (Supporting Information Figure S5).[27−30] By comparison, PNDI-T2 is an n-type alternating copolymer with low crystallinity. It orients face-on to the substrate, and absorbs strongly at 375 nm (Supporting Information Figure S5).[31−34] Demonstrating that both polymers can be patterned using the same tool and analyzed using the same predictive model shows the universality of the method. The Alvéole PRIMO (Figure 1a) was used for the photothermal patterning experiments. The assignment of good and poor solvents for each polymer was made after soaking the SP film in each of the solvents at room temperature. A good solvent will fully dissolve the SP and a poor solvent will not dissolve the SP at all at room temperature. For this study, 1,2-dichlorobenzene (DCB) and cyclohexanone (CHN) were chosen as the good and poor solvents respectively for P3HT. For PNDI-T2, *p*-xylene (XLN) and CHN were chosen as the good and the poor solvents respectively.

As discussed, photothermal lithography works on the principle that an SP will dissolve in a solvent mixture at some elevated temperature and all heating is achieved by using a focused laser. There are several process parameters that can affect the pattern shape and resolution like solvent quality (specific interactions with good and poor solvents and their ratio), polymer molecular weight (M_W), polymer polydispersity

https://doi.org/10.1021/acsapm.4c01884
ACS Appl. Polym. Mater. 2024, 6, 11302−11311

index (PDI), laser fluence (E_p), laser intensity, and dwell time. All of these process parameters effectively manipulate the temperature gradient in the SP film and locations at which a dissolution temperature (DT) is reached, which ultimately dictates the resulting pattern and dissolution rate. PDI of SPs is always greater than 1, so there is a range of temperatures over which the polymer dissolves in a solvent. DT_{start} is defined as the minimum temperature at which the polymer starts to dissolve into the solvent mixture. DT_{start} must be low enough that it can be quickly achieved by the thermal heating from the laser, and it must be high enough that SP does not dissolve into the solvent at room temperature, even after hours of solvent soaking.

Figure 1b shows a cartoon schematic of the experimental setup used to determine DT_{start}. The setup involves a solvent mixture contained in a well-mixed cuvette. The SP is coated on a substrate of known area and thickness which is immersed in the cuvette. We use a 405 nm 20 mW laser to probe the transmittance through the solvent, which tracks the amount of SP that dissolves into the solvent. We begin a slow (3 °C/min) temperature ramp from room temperature and slowly increase the temperature of the system. The transmittance through solvent decreases quantitatively as a function of the polymer solution concentration until the polymer is completely dissolved. The transmittance vs temperature plots for P3HT and PNDI-T2 can be found in the Supporting Information, Figures S2 and S3. Based on the DT_{start}, one could select the solvent concentration for patterning based on Figure 1c, which shows temperature versus good solvent volume fraction for P3HT and PNDI-T2. DT_{start} for PNDI-T2 in XLN + CHN is higher than that of P3HT in DCB + CHN. Therefore, to pattern at the same DT, the solvent ratio must be changed. The dashed lines are the solvent concentrations chosen for experimentation in this study, in the range 60−100 °C. In principle, the patterning rate would be increased by working at a lower DT_{start} because lower laser exposure time would be needed to produce a particular volume etch. However, since most semiconducting polymers have a PDI of 2−4, DT_{start} is usually about 30 °C lower than DT_{end} as seen in Figure 1c. The consequence of choosing a low DT_{start} is the systematic reduction of the SP layer thickness by dissolution of the shorter polymer chains.

The dissolution temperature experiment proves that polymer dissolution is driven by thermal stimulation alone. The purpose of the laser in photothermal patterning is to achieve precise micrometer-sized local heating. We have previously shown that there is no chemical reaction that occurs because of exposure to the laser.[35,36]

For the patterning experiment, an SP film was enclosed in a solvent cell with a 300 μm layer (<200 μL total solvent) of the solvent mixture. We then projected an image of the photomask (Supporting Information Figure S4) onto the surface of the SP and exposed it to a 375 nm laser (output power: ∼5.2 mW) embedded in the Alvéole PRIMO. It is important to note that P3HT and PNDI-T2 in solid state have significantly different absorbance at 375 nm based on the UV−vis-NIR spectra (refer to Supporting Information Figure S5). This further shows the universality of this process. We used a 20× objective lens to focus the photomask image on the SP layer. The area per projection was ∼0.17 mm^2 at this magnification. We used the P3HT results for the figures in this study but obtained similar results for both polymers. The experimental conditions for P3HT that were used are shown in Table 1:

Table 1. Experimental Conditions for P3HT

solvent concentration (%)	25%, 35%, and 45% DCB, rest CHN
laser fluence (in pJ/nm^2)	3, 5, 8 and 10
solvent cell orientation	"thru glass" and "thru solvent"
photomask width (in nm)	870, 1450, 2900, 3480, 4350, 5520 and 5800

The solvent cell assembly contains two glass pieces that enable laser exposure while enclosing the solvent to prevent leakage and human exposure. One glass is a thin (0.1 mm) coverslip, and the other is a standard 1 mm microscope slide or indium tin oxide (ITO) glass. We performed experiments with the SP coated onto either of the glass pieces, such that the polymer is always in contact with the solvent. This test is significant because the laser had to travel through different materials and distances to reach the polymer as shown in Figures 4b and 5b. The case in which the laser had to travel through glass alone to reach the polymer is referred to as the "thru glass" case and when the laser had to travel through the glass and the solvent to reach the polymer is called the "thru solvent" case. The choice of through glass or through solvent is consequential for the experiment design for two reasons. First, through solvent enables the use of a standard thickness substrate, but there are more optical interfaces and a larger working distance between the laser source and the SP layer. Thru glass requires only the use of a coverslip (0.1 mm thick) for the device substrate (delicate) but reduces the focal distance and removes reflectances off the interfaces. The other consequence is that the laser heats the glass/SP interface in the case of thru glass excitation, whereas it heats the solvent/SP interface in the thru solvent case. In the future, organic electronic devices are expected to be fabricated on flexible webs or metal foils with varying thicknesses. It is important that any patterning technology be compatible with all substrate geometries.

Figure 2 shows the line profiles of the patterns obtained for P3HT with 35% DCB + 65% CHN for both orientations, all four laser fluences, and seven different exposure widths. These line profiles are extracted from atomic force microscopy (AFM) images which can be found in Supporting Information, Figure S8. It is clear from Figure 2 that there are discernible etch shape and depth differences in the line profiles obtained for the two orientations and four fluences. As expected, increasing the laser fluence results in more heating and therefore deeper features. Also, the "thru solvent" orientation results in wider features. We model laser-induced heating and polymer dissolution into the homogeneous, well-mixed solvent to understand the effect of changing the processing parameters on the shape and dimensions of the patterns obtained. We also note that more polymer redeposition occurs in the "thru glass" orientation which results in positive features in the AFM image. Our model cannot account for the redeposition of polymer in locations far from the dissolution location. The "thru glass" sample has more redeposition because in this orientation, gravity pulls the particles down to the substrate. Future iterations of the sample cell will feature solvent flow to remove polymer from the system before redeposition for both orientations.

To further bolster the universality of photothermal patterning, we patterned a nonthiophene containing polymer. Poly(9,9-dioctylfluorene-alt-benzothiadiazole) (F8BT) is a popular fluorene copolymer that is used in organic light

https://doi.org/10.1021/acsapm.4c01884
ACS Appl. Polym. Mater. 2024, 6, 11302−11311

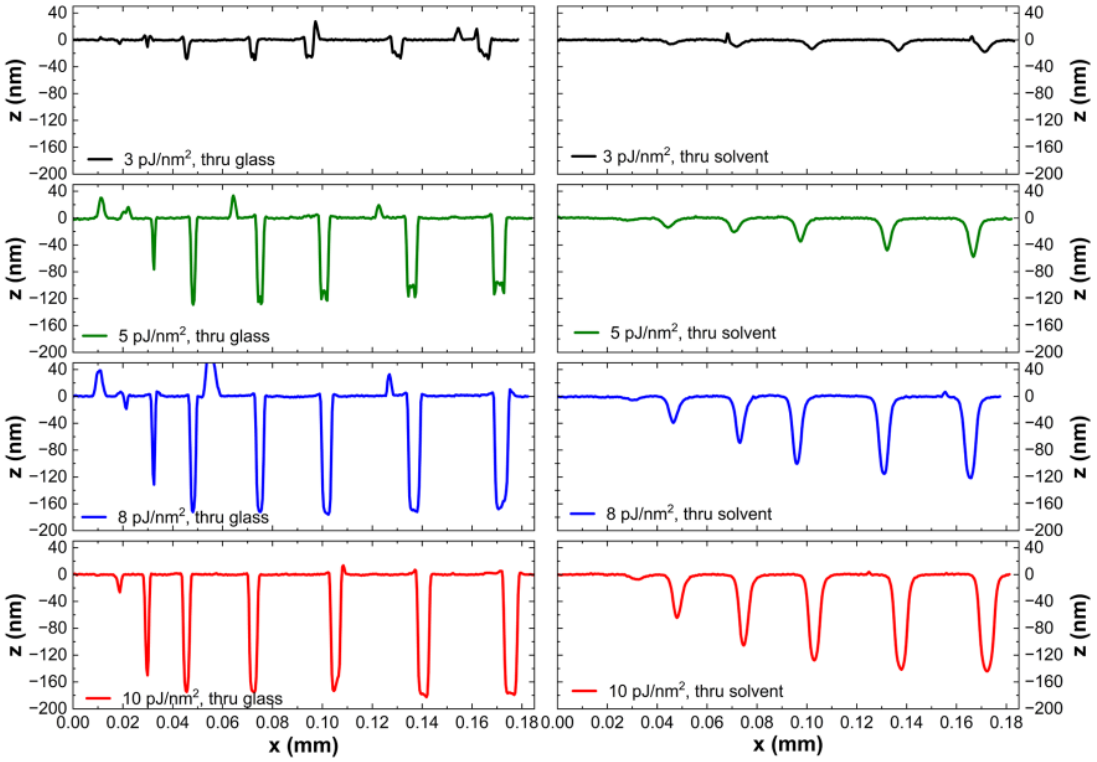

Figure 2. AFM cross sections of patterned P3HT with 35% DCB + 65% CHN. These line cuts are taken from AFM images (for full AFM images refer to Supporting Information Figure S5). Thru glass profiles are on the left, and thru solvent is on the right. The different profiles come from different exposure widths, and the different line colors come from different exposure intensities.

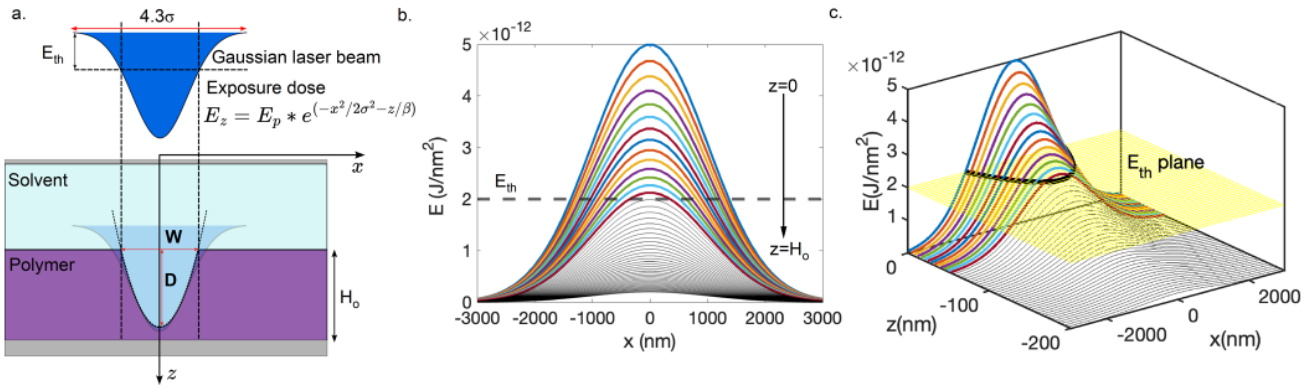

Figure 3. (a) Cartoon schematic of the patterning process "thru solvent" orientation. Not to scale. (b) Laser exposure dose $E(x, z)$ vs cross-section position x. (c) Three-dimensional (3-D) plot of $E(x, z)$ vs x and z with the threshold energy for dissolution (E_{th}) depicted.

emitting diodes. The details and results of patterning can be found in Supporting Information Section S5.

Predictive Model for Pattern Width and Depth. A practical prerequisite for this processing technique is a quantitative model that predicts feature geometry as a function of the processing variables. We introduced DT_{start} above, which is the temperature at which the polymer starts dissolving into the solvent. We also introduce a threshold energy (E_{th}), which is the cumulative optical power (in Joules per nm^2) that is needed to reach DT_{start}. Just like DT_{start}, E_{th} depends strongly on the choice of solvent mixture because the polymer will dissolve at a lower temperature in a better solvent, corresponding to a lower E_{th}. The dissolution occurs over a time scale of seconds to minutes, which allows us to describe the system as quasi-steady state.

To model this system, we start by assuming a Gaussian-shaped laser beam intensity profile projected onto the top surface of the polymer film. The SP film is in equilibrium with a solvent mixture, such that no dissolution occurs at room temperature. Initial absorption of photons from the laser results in heating of the polymer with a temperature distribution that is identical with the absorbance profile of the laser in the film. The polymer starts to dissolve into the solvent mixture when the local temperature exceeds DT_{start}. Figure 3a shows a cartoon schematic of the entire patterning process. A Gaussian laser beam distribution with characteristic width σ can be expressed as

https://doi.org/10.1021/acsapm.4c01884
ACS Appl. Polym. Mater. 2024, 6, 11302−11311

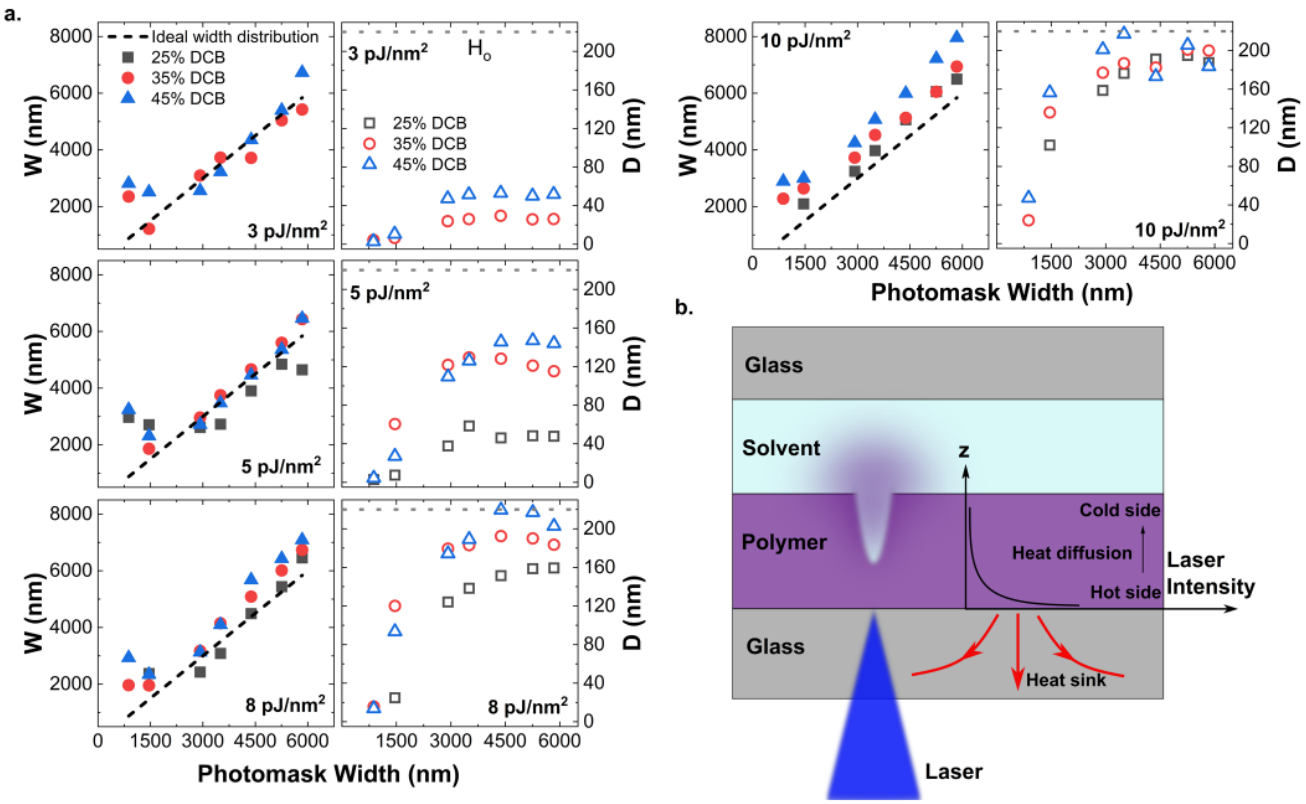

Figure 4. "thru glass" orientation: (a) Left panel is photomask width vs W and the right panel is photomask width vs D for P3HT at 3, 5, 8, and 10 pJ/nm^2. (b) Cartoon schematic describing the dissolution and temperature gradients in the SP.

$$E(x, z) = E_p \exp\left(-\frac{x^2}{\sigma^2}\right)\exp\left(-\frac{z}{\beta}\right) \quad (1)$$

where E_p is the peak exposure dose at $x = z = 0$. The beam intensity attenuates as it penetrates the film, described by an exponential decrease in the z-direction with a decay constant β that is related to the polymer extinction coefficient at the excitation energy.

We build on models of exposure profiles for a photoresist exposed to Gaussian laser function with an exponential decay.[37] For this, we define the contrast γ that quantifies the difference between the exposed and the unexposed region on the polymer:

$$\gamma = \frac{\frac{z}{H_o}}{\ln\frac{E(z)}{E_{th}}} \quad (2)$$

where H_o is the original height (or thickness) of the film and $E(z)$ is the optical field intensity. A larger γ indicates a larger observable difference between the exposed and unexposed areas.

Equations 1 and 2 can be rearranged in terms of spatial parameters x and z to obtain

$$z = \frac{\gamma H_o}{1 + \frac{\gamma H_o}{\beta}}\left[\ln\frac{E_p}{E_{th}} - \frac{x^2}{\sigma^2}\right] \quad (3)$$

which is a parabolic equation of the form of $A + Bx^2$. The parameter A can be solved in terms of the predicted etch feature depth (D) at the center position (as shown in Figure 3a) for the laser where:

$$D = A = \frac{\gamma H_o}{1 + \frac{\gamma H_o}{\beta}}\ln\frac{E_p}{E_{th}} \quad (4)$$

The predicted pattern width at the surface (W) is a combination of the parameters A and B. W is defined as the full width at $z = 0$ (as shown in Figure 3a):

$$W = 2x_o = 2\sqrt{\frac{A}{B}} = 2\sqrt{2}\sigma\sqrt{\ln\frac{E_p}{E_{th}}} \quad (5)$$

where x_o is the half of the top width of the obtained pattern at $z = 0$, and

$$B = \frac{\gamma H_o}{1 + \frac{\gamma H_o}{\beta}}\left(\frac{x^2}{\sigma^2}\right) \quad (6)$$

Solving for z in terms of D and W then yields the following depth profile.

$$z = -D + \left(\frac{4D}{W^2}\right)x^2 \quad (7)$$

The Gaussian laser intensity pattern yields a parabolic etch shape because the wings of the Gaussian do not exceed the E_{th} needed to start dissolution. This is depicted schematically in Figure 3b,c with representative plots of $E(x, z)$ vs x over the thickness (z) of the SP. The polymer dissolves into the solvent only if $E > E_{th}$. This is represented by the colored Gaussian spectra in Figure 3b,c. The parabolic etch shape is the intersection of the E_{th} plane (in yellow) with the Gaussians, corresponding to cases in which dissolution occurs.

https://doi.org/10.1021/acsapm.4c01884
ACS Appl. Polym. Mater. 2024, 6, 11302−11311

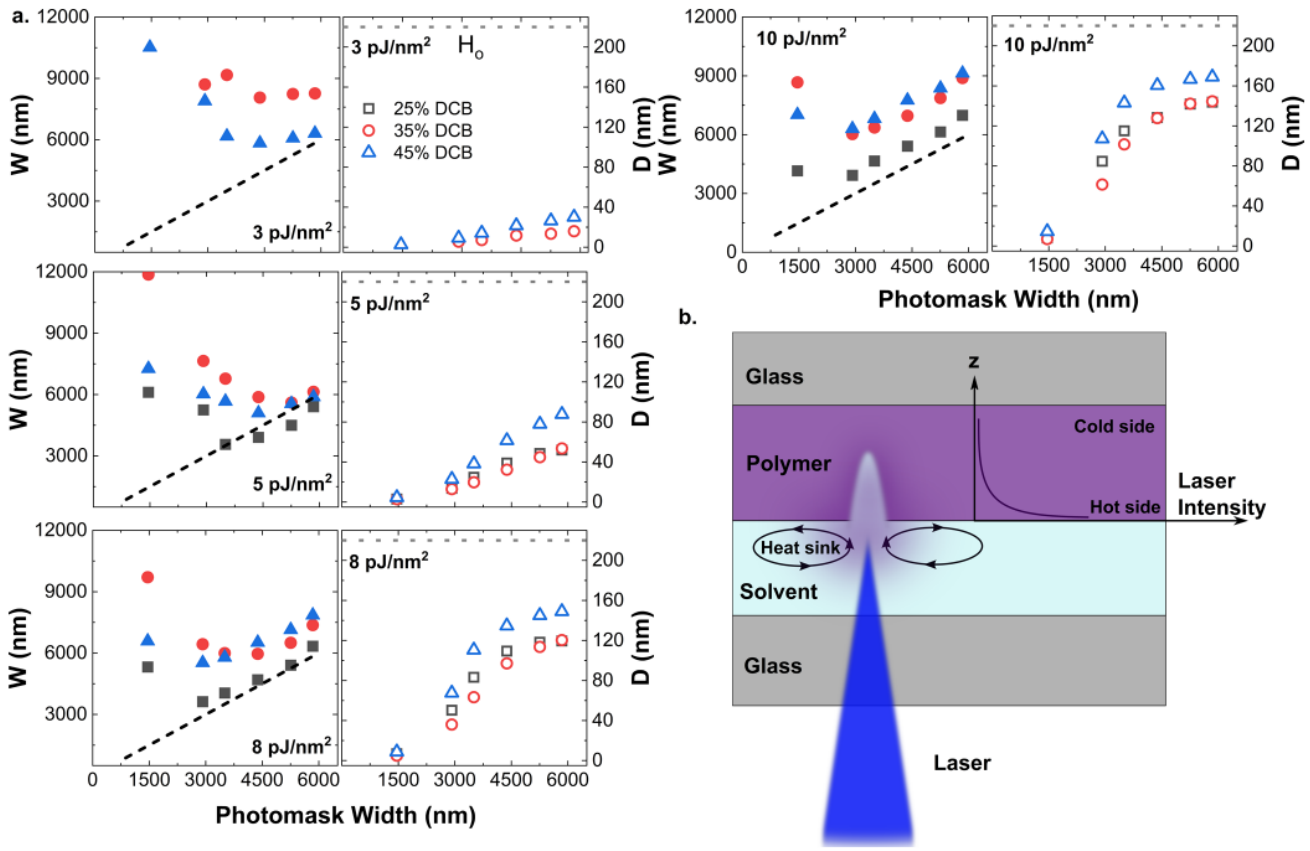

Figure 5. "thru solvent" orientation. (a) Left panel is photomask width vs W and the right panel is photomask width vs D for P3HT at 3, 5, 8, 10 pJ/nm^2. (b) Cartoon schematic describing the dissolution and temperature gradients in the SP.

We apply this model to fit patterns D and W from the measured AFM patterns. Figures 4a and 5a represent photomask width vs W and D for the "thru glass" case and "thru solvent" case respectively for P3HT. There is a clear systematic difference in W and D vs exposure intensity for the two different solvent cell orientations. These differences can be explained by differences in the thermal transport out of the SP film. We make the following assumptions to understand thermal transport effectively:

1 Glass is transparent at 375 nm. The polymer is the only optically absorbing material in the system.
2 Since light absorbs with exponential reduction in intensity with depth, the heat gradient must match the optical field intensity $E(x, z)$.
3 Laser orientation with respect to the film changes the thermal gradient as follows:
   - "thru glass" case: the glass−polymer interface is hotter than the solvent−polymer interface.
   - "thru solvent" case: the solvent−polymer interface is hotter than the glass−polymer interface.

For the "thru glass" orientation, W increases linearly with the photomask width for all fluences, while D saturates at ∼220 nm, which is the layer thickness (Figure 4a). Figure 4b is a cartoon schematic depicting the dissolution of the polymer into solvent- and laser-induced temperature gradients in the "thru glass" orientation. The laser heats the polymer most at the polymer−glass interface. P3HT is a poor conductor of heat (k = 0.158 W/mK), but glass acts as a heat sink (k ∼ 1.1 W/mK) pulling heat from the polymer film. As a result, the glass heats laterally and results in W that is wider than the photomask width (dashed line in the left panel of Figure 4a).

For this orientation, the 115 nm layer closer to the glass gets heated first (β ∼ 115 nm, calculation in Supporting Information S7). Heat diffuses slowly to the cold side which is the polymer−solvent interface but more quickly to the glass heat sink. Dissolution into the solvent must occur at the polymer−solvent interface. Since the glass heat sink is closer to the hot polymer interface in this case, vertical heat transfer in the z-direction is more efficient than lateral heat transfer in the x-direction, which results in lower W and higher D as compared to the "thru solvent."

Figure 5a shows the photomask width vs W and D for the "thru solvent" orientation. In this case, lower photomask widths result in a higher W. W decreases first and then increases again. This dip in W decreases with increasing fluence, and it eventually approaches linearity like in the previous case. D increases linearly with photomask width until 5 pJ/nm^2 and then saturates at higher fluences and at higher photomask widths. It is also clear that patterns are deeper in the "thru glass" case, which proves a difference in the heat transfer mechanism between the two cases. Figure 5b is a cartoon schematic describing the dissolution in the "thru solvent" orientation. The laser heats the polymer at the polymer−solvent interface. In this case, the hot side of the polymer is closer to the solvent, and the solvent serves two purposes, acting both as a heat sink and as a front for dissolution. The solvent convects in response to thermal gradients, resulting in a more significant lateral heat spread through the solvent compared with the "thru glass" case.

https://doi.org/10.1021/acsapm.4c01884
ACS Appl. Polym. Mater. 2024, 6, 11302−11311

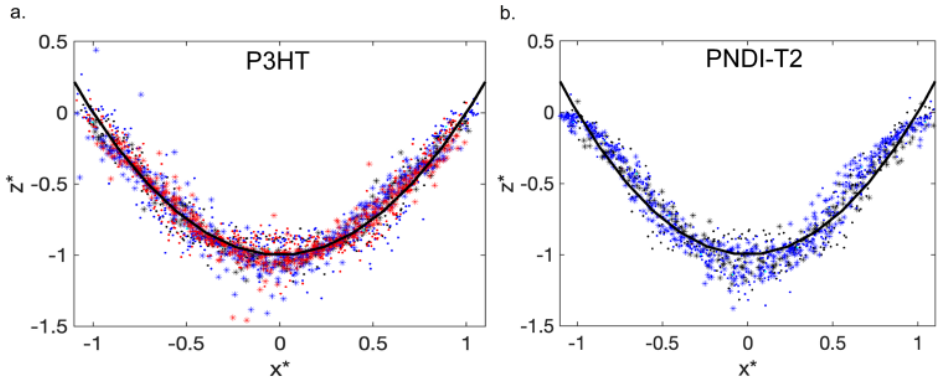

Figure 6. Master curves for (a) P3HT and (b) PNDI-T2 show data collapse across the entire range of operating conditions.

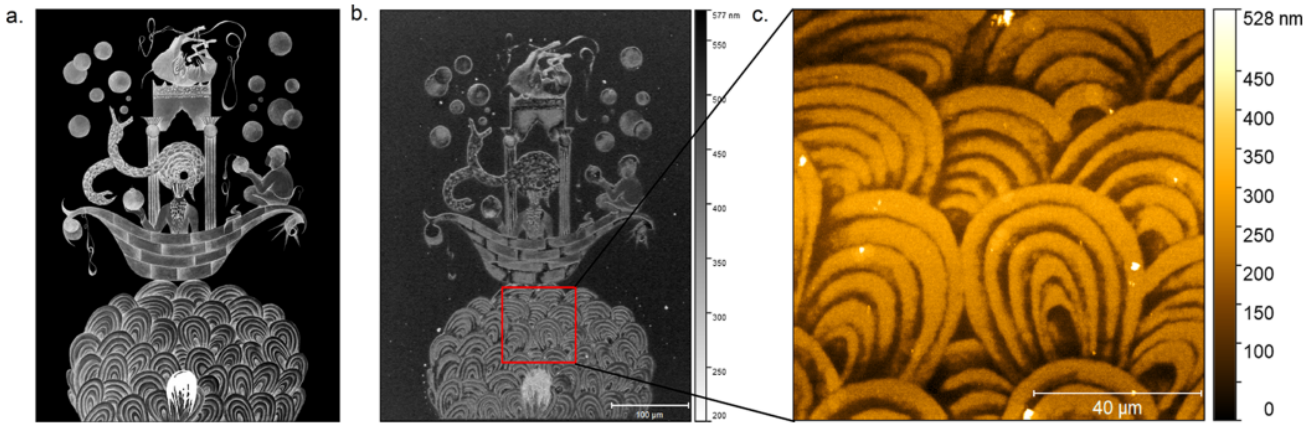

Figure 7. (a) Painting by Shiva Ahmadi used as a photomask for patterning P3HT. (b) Optical image of P3HT after patterning. (c) AFM image of the highlighted area on the optical image.

Solvent convection, which is not considered in the model, is likely the reason for higher W and lower D obtained in the "thru solvent" orientation. For a future scale-up of photothermal patterning, a solvent flow would enable the control of heat transport through the solvent layer.

Master Curve. We can use dimensionless variables to reduce the number of parameters in the model and to make the model readily generalizable to other processing conditions. In this case, we want to predict the W and D of a photothermally etched feature in SPs using only information like E_{th}, DT_{start}, DT_{end}, E_P, β, and time. We choose dimensionless variables

$$z^* = \frac{z}{A}, \quad x^* = \frac{x}{\sqrt{A/B}} \tag{8}$$

Substituting these into eq 7 yields

$$z^* = -1 + x^{*2} \tag{9}$$

We obtain a master curve for P3HT and PNDI-T2 by applying this nondimensional model to all AFM cross-section patterns for all widths, intensities, solvents, and operating conditions (Figure 6). The master curve collapses all data into a narrow range of values across the entire range of operating conditions. It is representative of the fact that any SP can be patterned with a combination of solvents and laser heating. The two curves are not identical, meaning that one cannot pattern PNDI-T2 under the same conditions as P3HT. The collapse of the data into one curve does demonstrate that all data under all conditions can be accurately described by the model for a particular polymer and that the model should be trusted to have predictive power outside the measured range, for example, for the same polymer in a different solvent mixture. Significantly more research will be needed to predict processing conditions for more polymers, but the success of this model shows that it can be used across all measurement conditions and with any polymer to predict the etch depth and width in the photothermal patterning of semiconducting polymers.

DEMONSTRATION OF DEPTH SENSITIVITY AND LARGE AREA PATTERNING

We also took this opportunity to demonstrate the capabilities of Alvéole PRIMO in the field of polymer patterning. We used Figure 7a as the photomask. This piece of art is made by Prof. Shiva Ahmadi from the Department of Art and Art History at University of California Davis. The size of the projected image on the surface of P3HT was 404 × 554 μm^2. The solvent mixture used was 45 vol % DCB, 55 vol % CHN. The image was broken into 256 gray scale intensities that scaled from below E_{th} to full depth etching of the P3HT film. Thus the gray scale of the image is recorded as a depth map or topo map of the image. Figure 7b is an optical image of patterned P3HT. All of the very detailed features of the artwork are present in the etched P3HT with no large scale distortions. There are some white specks on the image that come from redeposition of the polymer. We hope to remove this artifact in future

https://doi.org/10.1021/acsapm.4c01884
ACS Appl. Polym. Mater. 2024, 6, 11302−11311

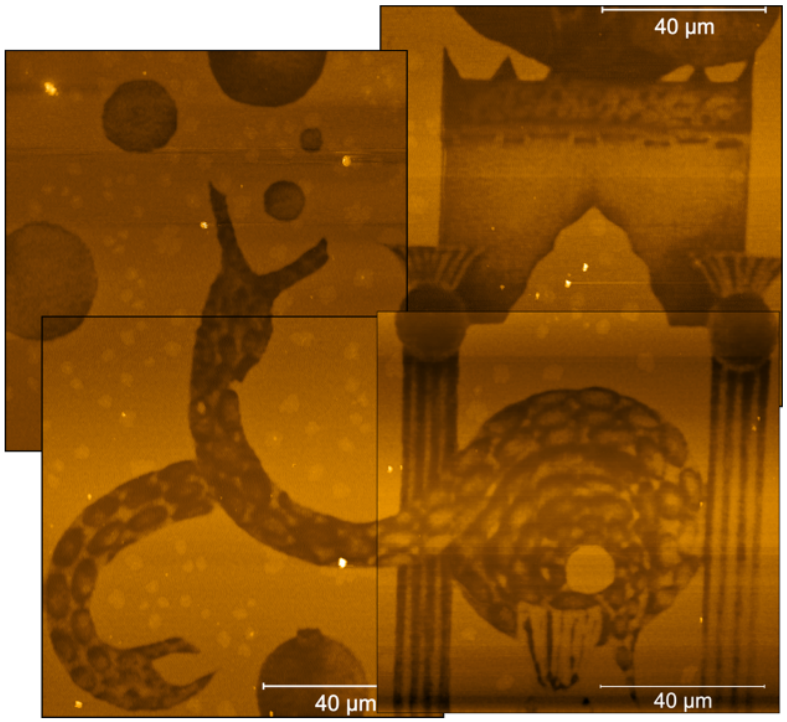

Figure 8. AFM images of patterned P3HT from Figure 7b are put together.

upgrades of the patterning apparatus. Figure 7c is an AFM image of the highlighted area in the optical image. We were able to achieve a resolution ∼2 μm with depth sensitivity of ∼10 nm (Supporting Information Section S8). The AFM images show that the gray scale image was perfectly transferred to the P3HT surface. This demonstrates that the polymer can be patterned over larger areas at sufficient resolution for device applications.

To make sure that the polymers maintain their opto-electronic properties after patterning, we conducted UV−vis spectroscopy and four-probe sheet resistance measurements on P3HT before and 2−3 h after patterning. The UV−vis spectra and conductivity measurements prove that opto-electronic properties of P3HT remain intact after patterning (for details refer to Supporting Information Section S6).

Figure 8 is a collage of AFM images of patterned P3HT from Figure 7b. This is an excellent demonstration of the resolution that Alvéole PRIMO is capable of achieving. The columns on the bottom right show parallel wires of P3HT with 5 μm width and hundreds of μm length. The dimensions of the image show the capability to pattern at the 1 μm resolution scale over dimensions of 1 mm.

CONCLUSIONS

In this article, we patterned P3HT and PNDI-T2 using photothermal lithography on a commercially available direct-write photolithography instrument, such as the Alvéole PRIMO. We developed a quasi-steady-state model to investigate the photothermal dissolution of SPs in solvent mixtures induced by a laser beam. We introduced parameters such as dissolution temperature and threshold energy to quantify the influence of solubility kinetics on heat transfer within the film. Through our analysis, we successfully determined the depth and width of the patterns obtained, tying feature size to the laser intensity, dwell time, and solvent quality for two different semiconducting polymers. By gaining a preliminary understanding of the heat transfer effects, we were able to identify the regime in which these effects dominate, thereby enabling us to modify the shape of the patterns obtained. We demonstrated that any polymer can be patterned over an area of mm^2 with a resolution of 1 μm. This research significantly contributes to the development of a cost-effective and rapid patterning technology for SPs, opening up possibilities for their industrial applications in the field of electronic devices.

MATERIALS AND METHODS

1. *Materials*: P3HT was purchased from Sigma Aldrich (MKCF1948) and PNDI-T2 was purchased from Ossila (M1201A4). Dichlorobenzene, xylene, and cyclohexanone were purchased from Sigma Aldrich. Borosilicate glass microscope slides (Fischer Scientific) cut to the required size were used as the substrates. All substrates were cleaned by ultrasonication in acetone, methanol, isopropyl alcohol, and deionized water for 10 min each. They were then dried with compressed N_2 and UV-ozoned for 20 min.
2. *Thin film preparation*: All polymer thin films used in this paper were spin coated in a N_2 glovebox. P3HT films were coated at 800 rpm for 90 s from a 25 mg/mL DCB solution and were 220 nm thick. PNDI-T2 films were coated at 1000 rpm for 90 s from a 20 mg/mL 4:1 chloroform/chlorobenzene solution and were 550 nm thick. F8BT films were coated at 400 rpm for 90 s from a 30 mg/mL chlorobenzene solution and were 100 nm thick. All films were annealed at 125 °C for 1 h on a hot plate after spin coating.

ASSOCIATED CONTENT

Supporting Information

The Supporting Information is available free of charge at https://pubs.acs.org/doi/10.1021/acsapm.4c01884.

https://doi.org/10.1021/acsapm.4c01884
ACS Appl. Polym. Mater. 2024, 6, 11302−11311

Dissolution temperature; photomask used; UV−vis spectra for P3HT and PNDI-T2; AFM height images and cross sections for P3Ht and PNDI-T2; calculation of decay constant β; demonstration of depth control (PDF)

AUTHOR INFORMATION

Corresponding Author

Adam J. Moulé − *Department of Chemical Engineering, University of California Davis, Davis, California 95616, United States;* orcid.org/0000-0003-1354-3517; Email: amoule@ucdavis.edu

Authors

Meghna Jha − *Department of Chemical Engineering, University of California Davis, Davis, California 95616, United States;* orcid.org/0000-0003-3701-3051

Joaquin Mogollon Santiana − *Department of Chemical Engineering, University of California Davis, Davis, California 95616, United States*

Megan L. Hong − *Department of Material Science and Engineering, University of California Davis, Davis, California 95616, United States*

Emily Vong − *Department of Chemical Engineering, University of California Davis, Davis, California 95616, United States*

Shiva Ahmadi − *Department of Art and Art History, University of California Davis, Davis, California 95616, United States*

Harishankar Manikantan − *Department of Chemical Engineering, University of California Davis, Davis, California 95616, United States*

Complete contact information is available at: https://pubs.acs.org/10.1021/acsapm.4c01884

Notes

The authors declare no competing financial interest.

ACKNOWLEDGMENTS

This research was funded by NSF Advanced Manufacturing award #2208009 including salary for M.J., J.M.S., and A.J.M. We would also like to thank UC LEADS for their support and salary for E.V. We thank Alvéole Instruments for loan of the PRIMO instrument to the Moulé group at UC Davis.

REFERENCES

(1) Kim, H.-J.; Kim, K.-J.; Kwak, D.-S. A case study on modeling and optimizing photolithography stage of semiconductor fabrication process. *Qual. Reliab. Eng. Int.* **2010**, *26*, 765−774.

(2) Akcalt, E.; Nemoto, K.; Uzsoy, R. Cycle-time improvements for photolithography process in semiconductor manufacturing. *IEEE Trans. Semicond. Manuf.* **2001**, *14*, 48−56.

(3) Martinez, V. M.; Edgar, T. F. Control of lithography in semiconductor manufacturing. *IEEE Control Syst. Mag.* **2006**, *26*, 46−55.

(4) *Photolithography Equipment Market Size, Share & Trends Analysis Report By Process (Ultraviolet UV, Deep Ultraviolet), By Light Source (Mercury Lamp, Fluorine Laser), By Wave Length, By End-users, By Region, And Segment Forecasts*; 2023−2030. Report ID: GVR-4−68040−134−2.

(5) Hadziioannou, G.; Malliaras, G. G. *Semiconducting Polymers: Chemistry, Physics and Engineering*; John Wiley & Sons, 2006.

(6) Lodha, A.; Singh, R. Prospects of manufacturing organic semiconductor-based integrated circuits. *IEEE Trans. Semicond. Manuf.* **2001**, *14*, 281−296.

(7) Dimov, I. B.; Moser, M.; Malliaras, G. G.; McCulloch, I. Semiconducting polymers for neural applications. *Chem. Rev.* **2022**, *122*, 4356−4396.

(8) Paleti, S. H. K.; Kim, Y.; Kimpel, J.; Craighero, M.; Haraguchi, S.; Müller, C. Impact of doping on the mechanical properties of conjugated polymers. *Chem. Soc. Rev.* **2024**, *53*, 1702 DOI: 10.1039/D3CS00833A.

(9) Xu, Y.; Zhang, F.; Feng, X. Patterning of conjugated polymers for organic optoelectronic devices. *Small* **2011**, *7*, 1338−1360.

(10) Guo, W.; Chen, J.; Ma, T.; Chen, Z.; Li, M.; Zeng, H.; Lu, J. Direct Photolithography Patterning of Quantum Dot-Polymer. *Adv. Funct. Mater.* **2024**, *34*, No. 2310338.

(11) Zschieschang, U.; Klauk, H.; Borchert, J. W. High-resolution lithography for high-frequency organic thin-film transistors. *Adv. Mater. Technol.* **2023**, *8*, No. 2201888.

(12) Chang, J. S.; Facchetti, A. F.; Reuss, R. A circuits and systems perspective of organic/printed electronics: Review, challenges, and contemporary and emerging design approaches. *IEEE J. Emerging Sel. Top. Circuits Syst.* **2017**, *7*, 7−26.

(13) Tsai, C. E.; Liao, M. H.; Chen, Y. L.; Cheng, S. W.; Lai, Y. Y.; Cheng, Y. J.; Hsu, C. S. Triarylamine-based crosslinked hole-transporting material with an ionic dopant for high-performance PEDOT:PSS-free polymer solar cells. *J. Mater. Chem. C* **2015**, *3*, 6158−6165.

(14) Png, R. Q.; Chia, P. J.; Tang, J. C.; Liu, B.; Sivaramakrishnan, S.; Zhou, M.; Khong, S. H.; Chan, H. S. O.; Burroughes, J. H.; Chua, L. L.; Friend, R. H.; Ho, P. K. H. High-performance polymer semiconducting heterostructure devices by nitrene-mediated photocrosslinking of alkyl side chains. *Nat. Mater.* **2010**, *9*, 152−158.

(15) Abdolmaleki, H.; Kidmose, P.; Agarwala, S. Droplet-based techniques for printing of functional inks for flexible physical sensors. *Adv. Mater.* **2021**, *33*, No. 2006792.

(16) Qiu, M. J.; Du, W. W.; Zhou, S. Y.; Cai, P. Z.; Luo, Y. W.; Wang, X. X.; Yang, R.; Zhao, J. J. Recent progress in non-photolithographic patterning of polymer thin films. *Prog. Polym. Sci.* **2023**, *142*, No. 101688, DOI: 10.1016/j.progpolymsci.2023.101688.

(17) Hu, S. Q.; Huan, X.; Liu, Y.; Cao, S. X.; Wang, Z. R.; Kim, J. T. Recent advances in meniscus-on-demand three-dimensional micro- and nano-printing for electronics and photonics. *Int. J. Extreme Manuf.* **2023**, *5*, No. 032009, DOI: 10.1088/2631-7990/acdf2d.

(18) Chen, X. Z.; Luo, Q.; Ma, C. Q. Inkjet-Printed Organic Solar Cells and Perovskite Solar Cells: Progress, Challenges, and Prospect. *Chin. J. Polym. Sci.* **2023**, *41*, 1439−6203, DOI: 10.1007/s10118-023-2961-z.

(19) Lemarchand, J.; Bridonneau, N.; Battaglini, N.; Carn, F.; Mattana, G.; Piro, B.; Zrig, S.; Noël, V. Challenges, Prospects, and Emerging Applications of Inkjet-Printed Electronics: A Chemist's Point of View. *Angew. Chem., Int. Ed.* **2022**, *61*, No. e202200166.

(20) Beedasy, V.; Smith, P. J. Printed electronics as prepared by inkjet printing. *Materials* **2020**, *13*, No. 704.

(21) Kusaka, Y.; Miyashita, K.; Ushijima, H. Extending microcontact printing for patterning of thick polymer layers: semi-drying of inks and contact mechanisms. *J. Micromech. Microeng.* **2014**, *24*, No. 125019.

(22) Wang, S. G.; Wang, Z. W.; Li, J.; Li, L. Q.; Hu, W. P. Surface-grafting polymers: from chemistry to organic electronics. *Mater. Chem. Front.* **2020**, *4*, 692−714, DOI: 10.1039/C9QM00450E.

(23) Murrey, T. L.; Mulvey, J. T.; Jha, M.; Fergerson, A. S.; Vong, D.; Soika, A.; Lorek, J.; Dolan, S. E.; Tiffany-Appleton, D. R.; Moulé, A. J. Approaching Rapid, High-Resolution, Large-Area Patterning of Semiconducting Polymers Using Projection Photothermal Lithography. *Adv. Mater. Technol.* **2022**, *7*, No. 2100812.

(24) Dema, A.; Rahgozar, S.; Siquier, L.; van Haren, J.; Wittmann, T. *Controlling Cell Shape and Microtubule Organization by Extracellular Matrix Micropatterning*; Springer, 2022; pp 467−481.

(25) Berkamp, S.; Daviran, D.; Smeets, M.; Caignard, A.; Jani, R. A.; Sundermeyer, P.; Jonker, C.; Gerlach, S.; Hoffmann, B.; Lau, K.; Sachse, C. Correlative Light and Electron Cryo-Microscopy Workflow Combining Micropatterning, Ice Shield, and an In-Chamber Fluorescence Light Microscope. *Bio-Protocol* **2023**, *13*, No. e4901, DOI: 10.21769/BioProtoc.4901.
(26) Ghagre, A.; Amini, A.; Srivastava, L. K.; Tirgar, P.; Khavari, A.; Koushki, N.; Ehrlicher, A. Pattern-based Contractility Screening (PaCS), a reference-free traction force microscopy methodology, reveals contractile differences in breast cancer cells. *bioRxiv* **2020**, 2020.
(27) Brinkmann, M. Structure and morphology control in thin films of regioregular poly (3-hexylthiophene). *J. Polym. Sci., Part B: Polym. Phys.* **2011**, *49*, 1218−1233.
(28) Himmelberger, S.; Duong, D. T.; Northrup, J. E.; Rivnay, J.; Koch, F. P.; Beckingham, B. S.; Stingelin, N.; Segalman, R. A.; Mannsfeld, S. C.; Salleo, A. Role of Side-Chain Branching on Thin-Film Structure and Electronic Properties of Polythiophenes. *Adv. Funct. Mater.* **2015**, *25*, 2616−2624.
(29) Nagamatsu, S.; Pandey, S. S. Ordered arrangement of F4TCNQ anions in three-dimensionally oriented P3HT thin films. *Sci. Rep.* **2020**, *10*, No. 20020.
(30) Tremel, K.; Ludwigs, S. *Morphology of P3HT in Thin Films in Relation to Optical and Electrical Properties*, P3HT Revisited-from Molecular Scale to Solar Cell Devices; Springer, 2014; Vol. *265*, pp 39−82.
(31) Luzio, A.; Martin, J.; Cheng, C. H.; Stingelin, N.; Toney, M. F.; Salleo, A.; Caironi, M. Improving molecular alignment and charge percolation in semiconducting polymer films with highly localized electronic states through tailored thermal annealing. *J. Mater. Chem. C* **2021**, *9*, 15848−15857.
(32) Vu, D.; Tang, L.; Thomsen, L.; Jevric, M.; Andersson, M. R.; McNeill, C. R. Formation and Charge Transport Properties of P (NDI2OD-T2) Thin Films with End-on Oriented Form III Crystallites. *Chem. Mater.* **2023**, *35*, 5550−5561.
(33) Kamatham, N.; Ibraikulov, O. A.; Durand, P.; Wang, J.; Boyron, O.; Heinrich, B.; Heiser, T.; Lévêque, P.; Leclerc, N.; Méry, S. On the Impact of Linear Siloxanated Side Chains on the Molecular Self-Assembling and Charge Transport Properties of Conjugated Polymers. *Adv. Funct. Mater.* **2021**, *31*, No. 2007734.
(34) Kim, J.; Ren, X.; Zhang, Y.; Fazzi, D.; Manikandan, S.; Andreasen, J. W.; Sun, X.; Ursel, S.; Un, H.-I.; Peralta, S.; et al. Efficient N-Type Organic Electrochemical Transistors and Field-Effect Transistors Based on PNDI-Copolymers Bearing Fluorinated Selenophene-Vinylene-Selenophenes. *Adv. Sci.* **2023**, *10*, No. 2303837.
(35) Jacobs, I. E.; Li, J.; Burg, S. L.; Bilsky, D. J.; Rotondo, B. T.; Augustine, M. P.; Stroeve, P.; Moulé, A. J. Reversible optical control of conjugated polymer solubility with sub-micrometer resolution. *ACS Nano* **2015**, *9*, 1905−1912.
(36) Jacobs, I. E.; Bedolla-Valdez, Z. I.; Rotondo, B. T.; Bilsky, D. J.; Lewis, R.; Ayala Oviedo, A. N.; Gonel, G.; Armitage, J.; Li, J.; Moulé, A. J. Super-resolution photothermal patterning in conductive polymers enabled by thermally activated solubility. *ACS Nano* **2021**, *15*, 7006−7020.
(37) Lee, E.; Hahn, J. W. The effect of photoresist contrast on the exposure profiles obtained with evanescent fields of nanoapertures. *J. Appl. Phys.* **2008**, *103*, No. 083550, DOI: 10.1063/1.2907971.